Iranian Journal of Chemistry and Chemical Engineering (IJCCE)

Affordable and efficient removal of Direct Red 16 from aqueous media based on nano zero-valent iron and nickel bimetallic nanoparticles supported on chitosan

Saghar Eftekhari[1], Mahmoud Reza Sohrabi[1], Saeid Mortezavi Nik[1]

[1]Department of Chemistry, North Tehran Branch, Islamic Azad University, Tehran, Iran

Abstract

Water pollution by azo dyes that are very toxic for living things is increasing rapidly. Thus, it is very important to eliminate these dyes from aqueous media. In this study, bimetallic nano zero-valent iron-nickel (nZVI-Ni) supported on biopolymer chitosan (CS-nZVI-Ni) were synthesized and characterized by scanning electronic microscopy (SEM), energy-dispersive X-ray spectroscopy (EDX), X-ray diffraction (XRD), Fourier-transform infrared spectroscopy (FTIR), Brunauer-Emmett-Teller (BET), and vibrating sample magnetometer (VSM). The synthesized nanocomposite was used as an adsorbent for the removal of Direct Red 16 (DR16) from the aqueous solution. The effect of pH (4-9), adsorbent dosage (0.08-0.3 g), contact time (5-30 min), and dye concentration (20-40 mg/L) revealed that the pH of 4, the adsorbent dosage of 0.2 g, contact time of 15 min, and initial concentration of 20 mg/L had maximum removal percentage (>96%). Two equilibrium models (Langmuir and Freundlich) were applied to calculate the adsorption parameters. The Langmuir model indicated the most suitable model that best fits the equilibrium data and the maximum adsorption capacity (q_{max}) was 84.74 mg/g with a coefficient of determination (R^2) value of 0.9993. The pseudo-second-order kinetic model fitted well for the adsorption of DR16 with R^2 of 0.9986. Thermodynamic parameters were calculated, and the results indicated that the adsorption was spontaneous and exothermic. The proposed adsorbent revealed excellent reusability with the removal efficiency from 88.32% to 60.28% after 5 cycles of adsorption experiments. Based on the results obtained from this work, the suggested adsorbent as a promising, simple, cost-effective, and efficient material could effectively be used for the elimination of various dyes from wastewater.

Keywords: *Bimetallic nanoparticles, Chitosan, Direct Red 16, Nickel, Zero valent iron*

1. Introduction

Water treatment has become one of the hot research topics because various pollutants are increasing due to their wide applications. Toxic dyes, heavy metal ions, pesticides, and nitroarenes are known as the main contaminants of wastewater. According to reports, the widespread use of organic dyes in various industries has caused them to be the major component of effluent [1]. The main use of dyes is in paper, rubber, plastic, textile, and wood industries. The principal pollutants released from industrial wastewater belong to dyes based on azo, anthraquinone, and triphenylmethane groups [2]. AZO dyes are the largest and most important group of dyes with the widest application in diverse industries. These dyes have one or more AZO groups (-N=N-) as a prominent feature that connects the two organic parts of the dye [3].

Direct Red (DR16) has been introduced as the most basic and widely used azo dye, which is a common pollutant of industrial wastewater. This dye is highly resistant under aerobic conditions and their anaerobic reduction renders aromatic amine by-products. Hence, Carcinogenic, mutagenic, and resistant to biodegradation are some of the negative effects of this dye. It poses serious risks to aquatic organisms and human life by impairing photosynthesis and inhibiting plant growth and entry into the food chain [4,5]. Also, a change in the pH and chemical composition of water occurs, which leads to an environmental imbalance and an enhancement in the chemical oxygen demand (COD) and biological oxygen demand (BOD) [6]. Therefore, it is necessary to remove these types of dyes from the water environment.

The remediation techniques such as electrocoagulation [7], coagulation [8], flocculation and precipitation flotation [9], electro-Fenton [10], oxidation [11], and advanced oxidation [12] have been reported to eliminate azo dyes. The limitations of these methods include costly, sludge production followed by disposal problems, use of electrical energy, and chemical reagents [13]. Sedimentation and coagulation–flocculation use a large number of coagulants and flocculants that produce huge amounts of sludge, which can be difficult to manage and needs extra procedures to treat. Electrocoagulation is a fast process for the treatment and it possesses very good removal efficiency of ionic and colloidal matter, as well as its electrode cost is relatively low, while it requires high energy demand, and it represents low cost-efficiency. Minimum sludge production and economically feasible are the strengths of the electro-Fenton method, while slow generation of H_2O_2, low current efficiency at a pH lower than 3, and lethargic Fe^{2+} regeneration are the limitations of this method [14,15]. Compared with the mentioned approaches, adsorption is widely accepted for the treatment of wastewater owing to its easy operation, cost-effectiveness, simple operation, high efficiency, more compatible with the environment, and easy recovery and reuse of adsorbents. The adsorption capacity of the adsorbent has a significant effect on the removal of pollution [16-18].

Wastewater containing azo dye can degrade using zero-valent metals due to their reducibility. The loss of stable azo bonds occurs through redox with active metals. Among them, zero-valent iron (ZVI) is of great interest due to its unique features such as being environmentally friendly, good reducibility, low-cost, and useful application for wastewater treatment [19]. Nano zero-valent iron (nZVI) particles can act as a strong electron donor for the oxidation and conversion of a wide range of contaminants. The high reactivity of nZVI compared to ZVI is usually attributed to the larger surface area and more surface reaction sites [20]. Also, the magnetic adsorbent can be easily separated from the solution by applying an external magnet [21]. However, nZVI particles have high magnetism and surface energy, which lead to easy aggregation and oxidation, as a result, their dispersion and

applications are reduced. Also, when interacting with water, a passive layer is formed, adversely affects the reactivity and transport capacity of nZVI [22]. Hence, as a successful approach, a second metal, such as nickel (Ni), can be integrated with nZVI to aid in stability while increasing the degradation rate compared to nZVI alone, resulting in effective dye removal [23-25]. Nickel with catalytic effect can cause better stability against corrosion and lower cost for site remediation. Iron-based bimetallic nanoparticles remain more stable in the air by this catalyst, which means it prevents oxidation. In comparison with other catalytic metals, Ni is less toxic and economically feasible [26,27].

Highly active surfaces metal nanoparticles (NPs) have highly active surfaces that lead to their aggregation. To avoid aggregation, the deposition of metal NPs on the supporter material like chitosan, silica, zeolite, alumina, and so on is a proper method [28]. Chitosan (CS) is widely chosen as a supporter due to its availability, nontoxicity, low cost, biodegradability, and unique structure [29]. By deacetylating chitin, CS as a linear copolymer is produced. Its advantages for the wastewater treatment include high adsorption capacity, floc formation, antimicrobial features, and renewable resources [30]. Most important of all these, the present reactive hydroxyl and amine groups in the CS structure make it a versatile candidate for the removal of dyes [31]. The high water solubility of CS leads to the effective removal of azo dyes using bimetal-CS without significant shaking and energy consumption [32].

The other adsorbents have been used for the removal of dyes and heavy metals. Neolaka et al., reported the removal of methyl red from an aqueous solution using Bali cow bones with a capacity of 7.2 mg/g [33]. Khera et al., used *Archontophoenix alexandrae* for the removal of copper, zinc, and nickel ions with capacities of 45.5, 30.0, and 25.0 mg/g, respectively [34]. Kuncoro et al., represented the adsorption of Cd^{2+} and Pb^{2+} from aqueous solution by a mixture of bagasse-bentonite with a capacity of 20.61 and -4.28 mg/g at a time of 45 min [35,36]. In the other study, Kuncoro et al., reported the removal of Pb^{2+} from an aqueous solution using a mixture of algae waste-bentonite at a contact time between 10 to 240 min [37].

The objective of this study was to treat aqueous solutions from azo dye, DR16, using bimetallic nZVI-Ni stabilized on CS as an environmentally friendly and economical adsorbent. The synthesized CS-nZVI-Ni was characterized by SEM, EDX, XRD, FTIR, DLS, and BET. The influences of some experimental variables (pH, adsorbent dosage, reaction time, and pollutant concentration) were evaluated on the removal percentage. To ascertain the maximum adsorption capacity (q_{max}) of the adsorbent, adsorption isotherms, including Langmuir and Freundlich for DR16 dye removal were investigated. Also, Pseudo-first-order, pseudo-second-order, and Elovich kinetic models were studied. The short removal time with high q_{max} and high removal percentage of the proposed adsorbent makes it remarkable compared to previous studies. Therefore, it can be used to remove DR16 dye and other dyes in the wastewater of various industries.

2. Materials and methods

2.1. Materials

Chitosan with a deacetylation degree between 75% to 85% and medium molecular weight was provided from Sigma-Aldrich. Iron(II) chloride tetrahydrate ($FeCl_2.4H_2O$), sodium borohydride ($NaBH_4$), nickel(II) sulfate ($NiSO_4$), hydrochloric acid (HCl), sodium hydroxide (NaOH), and acetone (C_3H_6O) were procured from Merck,

as well as DR 16 dye (Scheme 1) was purchased from Alvan Sabet Company (Iran, Tehran). Its molecular structure is related to the double azo class with a molecular weight of 637.55 g/mol.

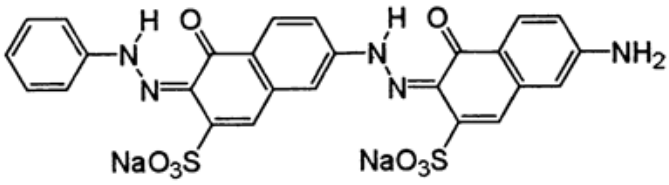

Scheme 1. Chemical structure of DR16

2.2. Preparation of CS-nZVI

200 mL of distilled water was deoxygenated under N_2 gas for 10 min using a mechanical stirrer at a rate of 354 rpm. Afterward, $FeCl_2.4H_2O$ (2g) and CS (0.4 g) were added 5 min apart. This mixture was dissolved well through a mechanical stirrer for 15 min under N_2 gas (solution 1). A certain amount of $NaBH_4$ (1g) was dissolved in 100 mL distilled water (solution 2). Solution 2 was poured into solution 1 drop by drop using a burette. This mixture was stirred for 15 min under N_2 gas, and then the filtration was accomplished via a vacuum pump. The obtained precipitate was transferred to another container and coated with acetone to prevent iron oxidation.

2.3. Preparation of CS-nZVI-Ni

$NiSO_4$ (0.09 g) was dissolved in 200 mL of distilled water and it was stirred for 10 min under N_2 gas. After that, a certain amount of CS/nZVI (2g) from the previous step was added to this solution and stirred for 15 min under N_2 gas. This mixture was filtered using a vacuum pump.

2.4. DR16 removal

Various concentrations of DR16 (20, 25, and 30 mg/L) were prepared at a constant pH of 4. Afterward, adsorbent dosage of 0.2 g was added to each container. The samples were stirred for 15 min, and then sampling was carried out. Followed by a strong magnet was used to take out the adsorbent. The solution was centrifuged for 10 min at 2000 rpm and the absorption of the supernatant solution was recorded by UV-Vis spectrophotometer (SU-6100 double beam). Based on Eq (1), the dye removal percentage was determined.

$$Removal\ (\%) = \frac{C_0 - C_e}{C_0} \times 100 \qquad (1)$$

Herein the initial and the final concentration of the DR16 are denoted by C_0 (mg/L) and C_e (mg/L), respectively [38].

3. Results and discussion

3.1. Characterization

3.1.1. SEM and EDX analysis

The surface morphology of CS-nZVI and CS-nZVI-NI was studied using ZEISS SEM (SIGMA VP, Germany) (Fig 1). The small white dots can be attributed to the placement of nZVI on CS. This image also represented that

nZVI was dispersed in the form of spherical particles on the surface of CS and A relatively smooth surface can be observed (Fig 1a). The excellent performance of CS resulted in good dispersion of nZVI and Ni on CS (Fig 1c). These metal NPs covered the surface of CS due to the presence of NH_2 and OH groups in the CS chain [29]. CS as a stabilizer can reduce the potential of the electrostatic barrier and stabilize the NPs. Also, it can improve the surface of NPs [26].

SEM equipped with an EDX detector (LEO 9121413) was used to analyze elements in the structure of CS-nZVI and Cs-nZVI-Ni (Fig 1b and Fig 1d). The presence of iron (Fe) and carbon (C) with the amounts of 70.62% and 24.36% confirms the formation of nZVI-CS. The existence of sodium (Na) in a small amount (5.02%) may be due to the use of NaOH during the synthesis process (Fig 1b). The Fe (65.54%) and Ni (25.35%) elements observed in Fig 1 (d) are assigned to the presence of nZVI and Ni in the structure of CS-nZVI-Ni. S with a weight of 9.11% was also detected, which was owing to the usage of $NiSO_4$ in the synthesis of CS-nZVI-Ni.

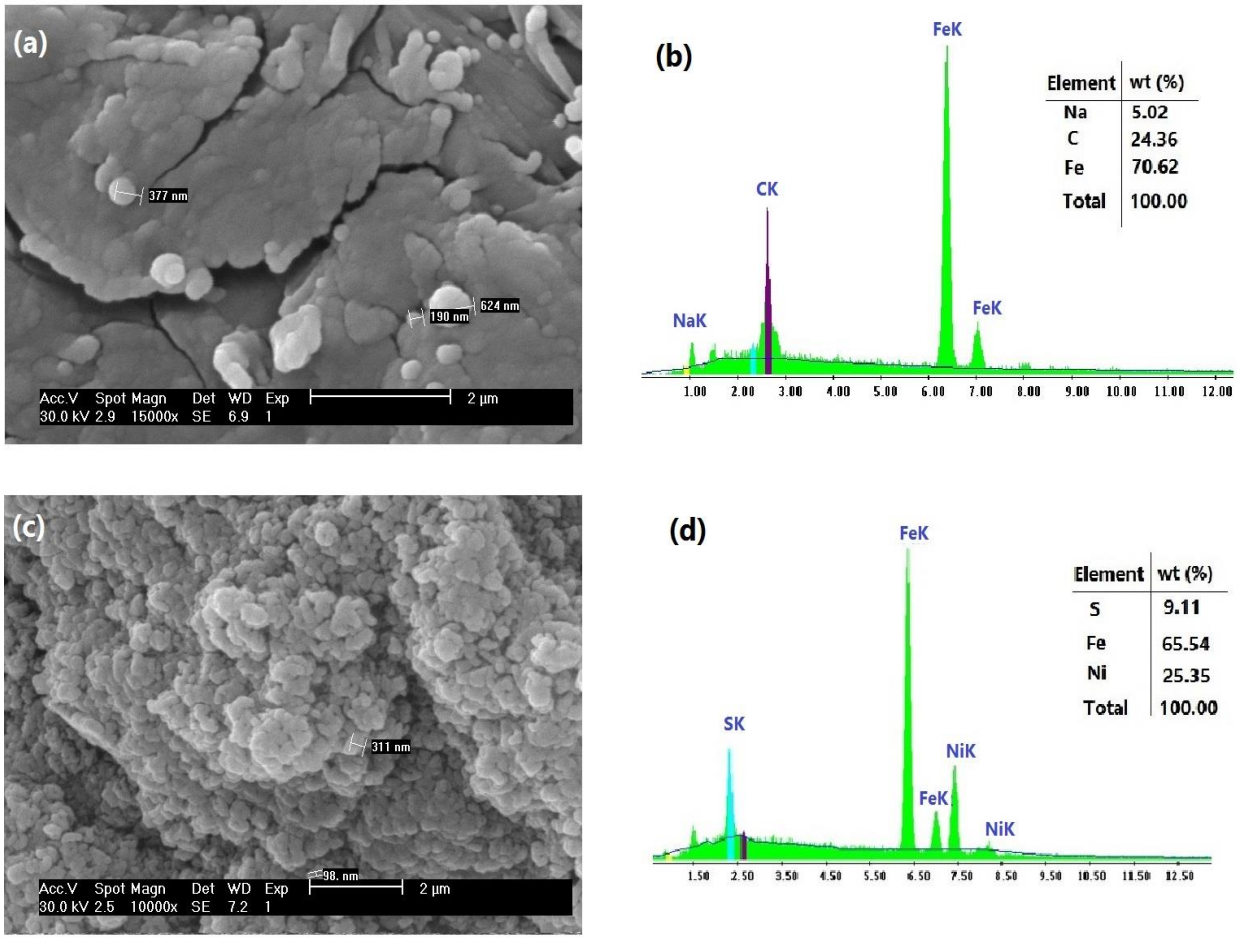

Fig 1. SEM images of (a) CS-nZVI and (c) CS-nZVI-Ni, EDX spectra of (b) CS-nZVI and (d) CS-nZVI-Ni

3.1.2. FTIR analysis

The functional groups of CS, CS-nZVI, and CS-nZVI-Ni were determined by Spectrum Two FTIR (Perkin Elmer). Fig 2 (a) displays the FTIR spectrum of CS. The stretching vibration of O-H and N-H is represented by a broad peak at 3435 cm^{-1} [39]. The absorption peak at 2925 cm^{-1} is assigned to the C-H stretching vibration of CH_2 [29]. The bending vibration related to the N-H can be observed at 1624 cm^{-1} [40]. The bands at 1375 and 1061 cm^{-1} are

related to the C–O stretching of the primary alcohol group and the C–O stretching of the polysaccharide bond, respectively [41]. The -CH and -CH_2 bending vibrations are detected at 892 cm^{-1} [42].

The FTIR spectrum of CS-nZVI (Fig 2b) shows the same peaks observed in CS with a small shift. So, it can be said that there is an interaction between iron and functional groups in CS, including amine and hydroxyl. The Fe–O stretching vibration appeared at 569 cm^{-1} [40].

In the FTIR spectrum of CS-nZVI-Ni (Fig 2c), the wavenumber of O-H and N-H was reduced, indicating the interaction between nZVI and Ni with bonds in the structure of the polymer [26]. The observed peak at 611 cm^{-1} is ascribed to the Ni–O stretching band [43].

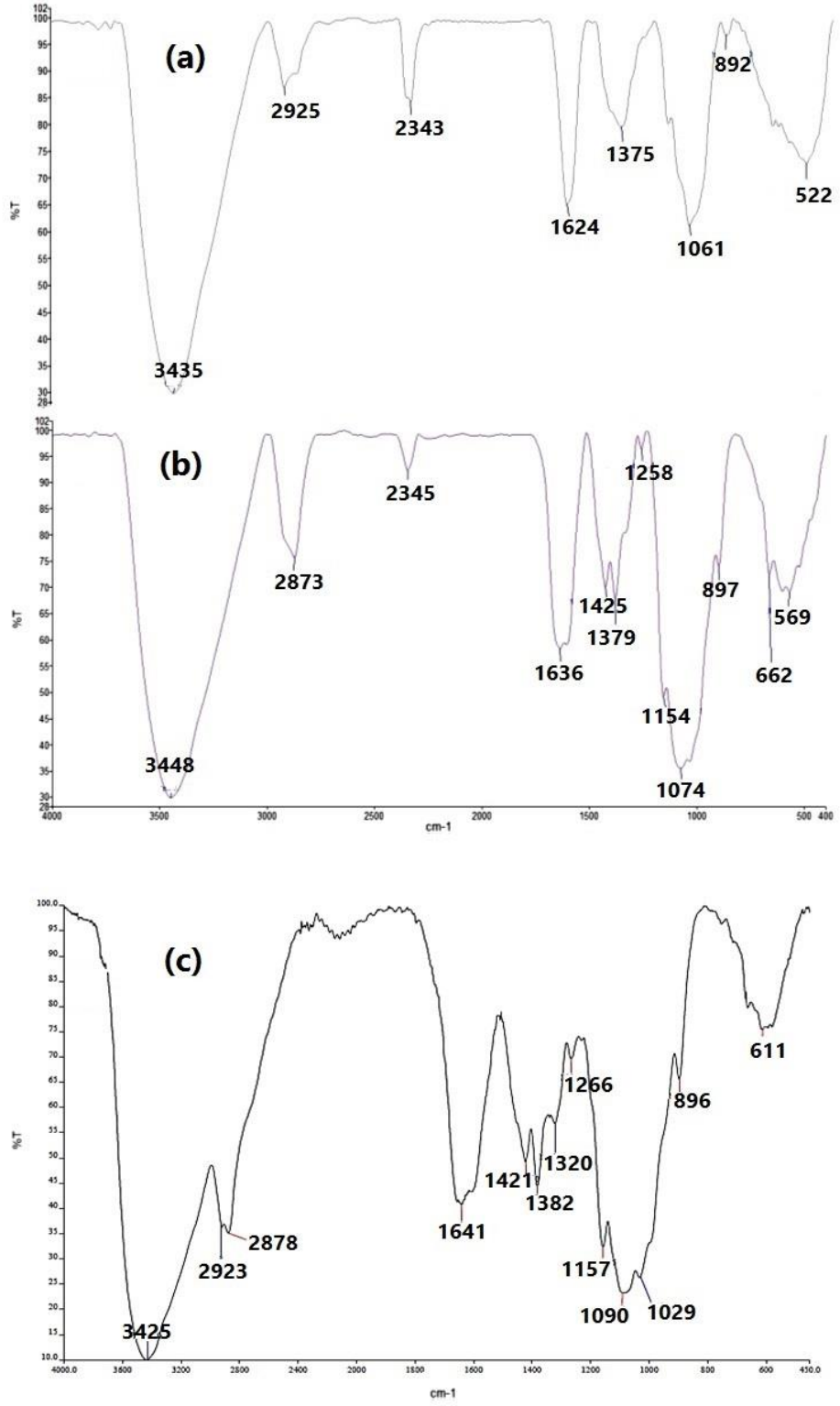

Fig 2. FTIR spectra of (a) CS, (b) CS-nZVI, and (b) CS-nZVI-Ni

3.1.3. XRD and DLS analysis

Panalytical XRD (Xpert Pro) with a Cu kα radiation source at the wavelength (λ) of 1.54 Å (0.154 nm) was used to analyze the crystalline structure of CS-nZVI and CS-nZVI-Ni. The data were achieved in 2θ range of 10° to

80° at a scan step time of 1 s at a temperature of 25°C. Fig 3 (a) illustrates the pattern of CS-nZVI. An amorphous peak around 2θ=20º can be ascribed to CS. The presence of iron particles was confirmed by a sharp peak at 2θ=35.82º. The pattern spectrum of CS-nZVI-Ni is shown in Fig 3 (b). The appearance of peaks at 20.07º and 36.30° (ICSD 631728) are assigned to the CS and Fe_2O_3, respectively [40,44]. According to JCPDS file no. 04–0850, A peak at 2θ=43.55° is related to the Ni with (111) plane [45]. Two peaks at 47.11º and 62.82º are related to the iron particles [46,47].

The crystalline size of the NPs was calculated using the Debye Scherrer equation (Eq 2).

$$D = \frac{K\lambda}{\beta cos\theta} \quad (2)$$

where K is the Scherer constant (between 0.9 to 1); the wavelength of the X-ray source is described by λ; β is the full width of the half maximum related to the diffraction peak; and θ shows the Bragg's angle [48]. The crystalline size of CS-nZVI-Ni was found to be 8.55 nm.

As shown in the size distribution histogram of dynamic light scattering (DLS), the average size of CS-nZVI-Ni was about 10 nm (Fig 3c).

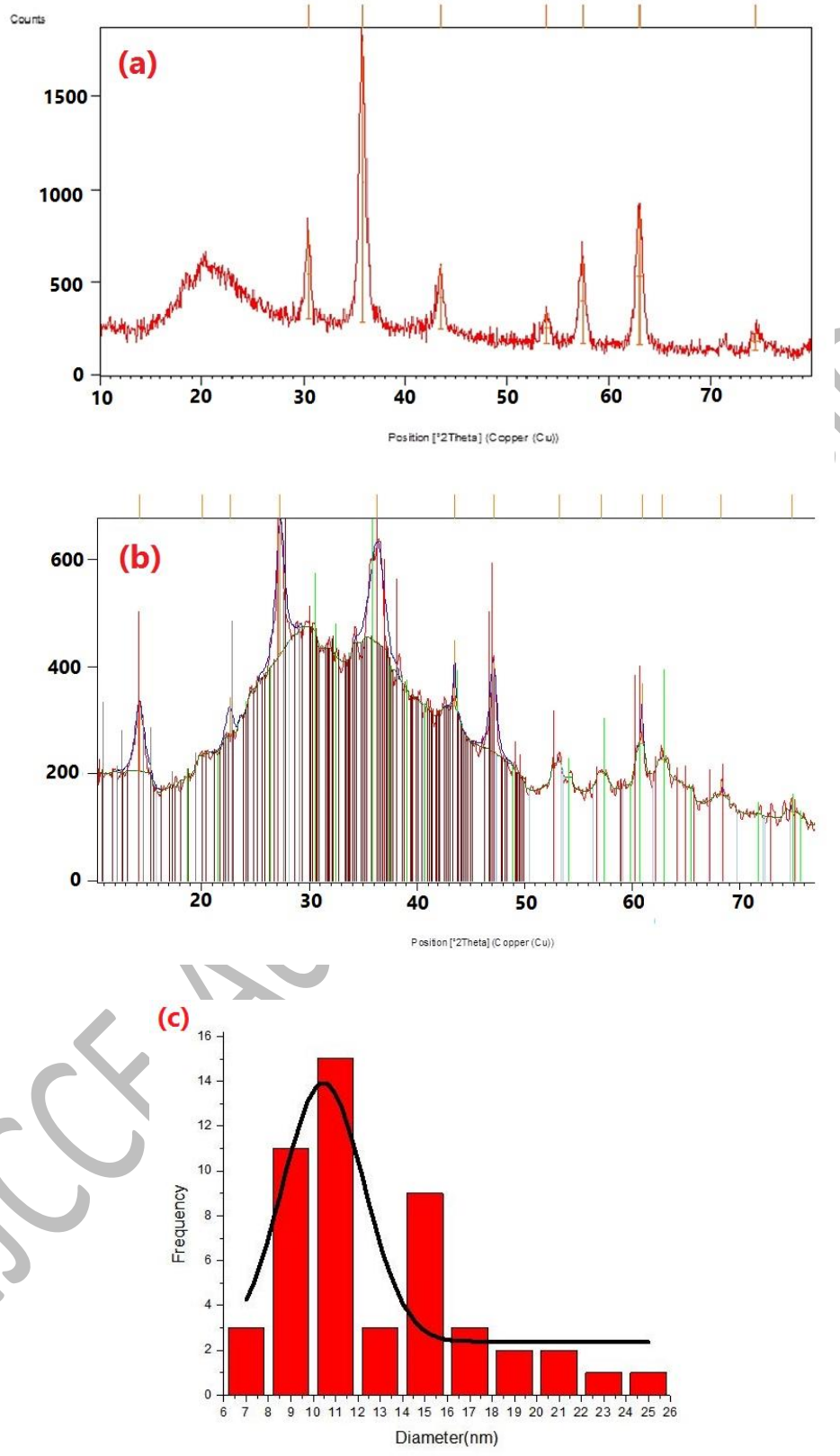

Fig 3. XRD pattern of (a) CS-nZVI and (b) CS-nZVI-Ni, and (c) histogram with size distribution of Cs-nZVI-Ni

3.1.3. BET analysis

The BET theory is close to the Langmuir theory, which specifies the specific surface area (SSA). This theory assumes that in multi-layer adsorption, equilibrium is established in all layers. Eq (2) describes the BET model.

$$\frac{P/P_0}{n\,(1-\frac{P}{P_0})}=\frac{1}{n_m C}+\frac{C-1}{n_m C}(P/P_0) \qquad (2)$$

where n is a certain amount of the adsorbed gas at the relative pressure P/P_0; n_m is the capacity of the monolayer of adsorbed gas; P denotes the pressure; P_0 represents the saturation pressure of a substance being adsorbed at the adsorption temperature; and C is BET constant [49].

Specific surface area and pore size distribution of CS-nZVI and CS-nZVI-Ni were determined by BET (Belsorp mini). The N_2 adsorption–desorption isotherm related to the CS-nZVI and CS-nZVI-Ni is shown in Fig 4 (a) and (c). The hysteresis loop of this figure matched with IUPAC classifications of physisorption isotherms (type IVa curve) [50]. Fig 4 (b) and (d) indicate the BET plots of CS-nZVI and CS-nZVI-Ni with R^2 of 0.9983 and 0.9998, respectively. These plots can estimate the BET surface area, which was obtained at 23.42 and 19.35 m^2/g for CS-nZVI and CS-nZVI-Ni, respectively. The Langmuir isotherm calculate specific surface area. The sharpness of the knee of the hysteresis loop was confirmed by the high value of parameter C (453.18). Table 1 represents BET and Barrett-Joyner-Halenda (BJH) BJH-dependent parameters. The average pore diameter of the adsorbent was found to be 15.62 nm, so it can be said that the CS-nZVI-Ni is mesoporous.

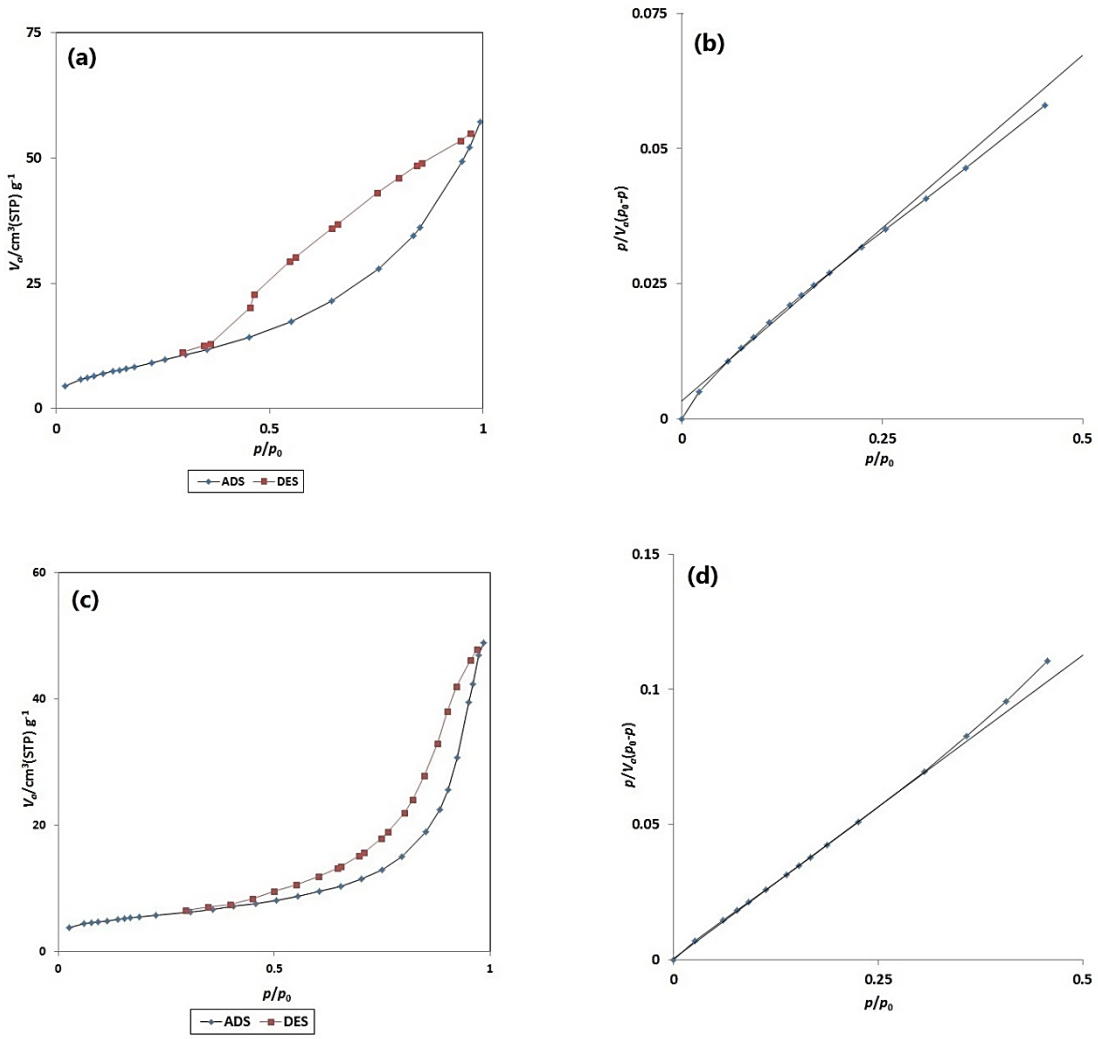

Fig 4. (a) and (c) nitrogen adsorption–desorption isotherm plot of CS-nZVI and CS-nZVI-Ni, respectively, (b) and (d) BET plot of CS-nZVI and CS-nZVI-Ni, respectively

Table 1. The data obtained from BET and BJH methods for the CS-nZVI and CS-nZVI-Ni

Sample	$a_{s,BET}$ (m^2/g)	$r_{p,peak}$ (Area) (nm)	V_p (cm^3/g)	a_p (m^2/g)	V_{total} (cm^3/g)
CS-nZVI	23.42	4.91	0.0795	25.86	0.0872
CS-nZVI-Ni	19.35	5.29	0.0740	20.17	0.0756

3.1.4. VSM analysis

Fig 5 shows the magnetic intensity of the Cs-nZVI-Ni nanocomposite. The saturation magnetization (σ_s) of the adsorbent was found to be 10.196 emu g^{-1}. Due to the combination of nZVI with CS, the magnetic properties may be slightly reduced.

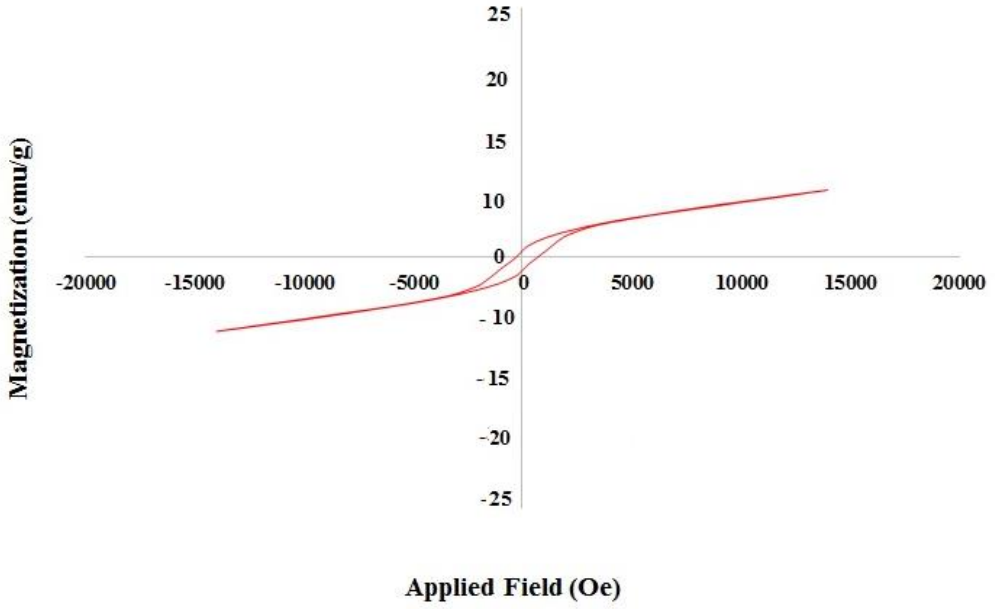

Fig 5. VSM image of CS-nZVI-Ni nanocomposite

3.2. Effect of operational parameter on dye removal

3.2.1. Effect of pH

According to Fig 6 (a), the pH change from 4 to 9 led to a decrease in the removal percentage from 96.21% to 71.18%. The anionic nature of DR16 and the negative surface charge of CS-nZVI-Ni can be a reason to justify this issue. In an acidic medium, positive ions neutralize these negative charges, providing the opportunity for DR16 molecules to get close to the CS-nZVI-Ni surface and adsorb on reactive sites. In contrast, repulsion is dominant in an alkaline environment, which leads to preventing the reaction of dye molecules with the adsorbent surface [4,5]. Hence, a pH of 4 with a removal percentage of 96.21% was selected as the best pH. In addition, the pH_{ZPC} of the CS-nZVI-Ni was determined by mixing a certain amount of adsorbent (0.2 g) and NaCl. The solution pH was adjusted to the required pH in the range of 4–8 using HCl and NaOH [51,52]. The pH_{ZPC} of CS-nZVI-N was obtained at 5.6

3.2.2. The effect of adsorbent dosage

The influence of adsorbent dosage was investigated in three different values (0.08 g, 0.14 g, 0.2 g, 0.3 g). As shown in Fig 6 (b), the maximum removal percentage (97.43 %) was related to the 0.2 g CS-nZVI-NI. This result emphasizes the issue that the enhancement in dosage of CS-nZVI-Ni increases the removal efficiency of DR16 to a large extent. When adsorbent dosage with small particle size is increased, the total total active surface available for dye adsorption is elevated, which causes more DR16 to be removed [53].

3.2.3. Effect of contact time

Fig 6 (c) denotes the effect of contact time at six various time intervals of 5 min on the DR16 removal. The dye removal efficiency was obtained at 97.64 % by CS-nZVI-Ni within 15 min. This may be due to the presence of enormous empty active sites on the surface of CS-nZVI-Ni. As the DR16 molecules were adsorbed onto the adsorbent surface, the availability of active sites diminished gradually, and the adsorbent became saturated, leading to a reduction in the rate of removal percentage in DR16 with time [53].

3.2.4. The effect of initial concentration

The impact of DR16 concentrations on the removal efficiency was assessed at concentrations ranging from 20 to 40 mg/L. As shown in Fig 6 (d), the increment of the DR16 concentration possesses a negative influence on the removal percentage. At high concentrations of dye, the surface of CS-nZVI-Ni was saturated with DR16, which caused a decrease in the uptake and finally decline in removal percentage [54]. Therefore, a concentration of 20 mg/L with a removal percentage of 98.59% was selected as the best value.

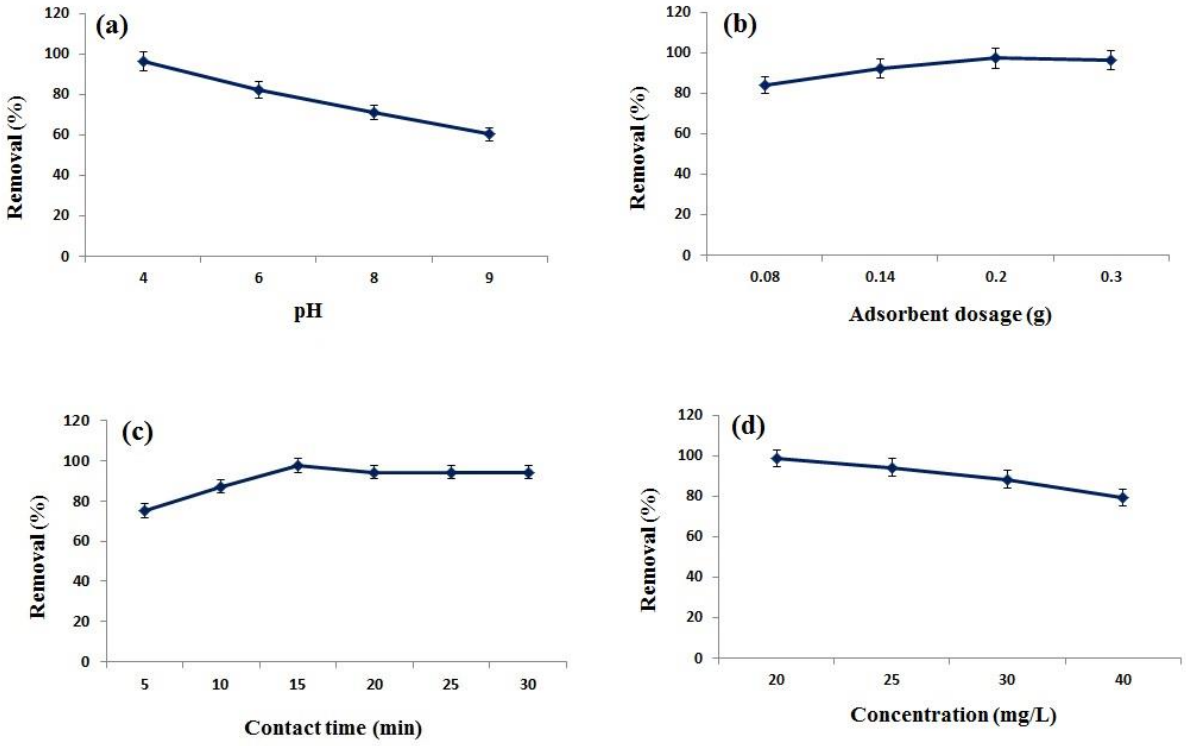

Fig 6. The effect of (a) pH, (b) adsorbent dosage, (c) contact time, and (d) initial concentration on the removal percentage of DR16 with 3 repetitions

3.3. Adsorption isotherm

Two most widely used adsorption isotherm models i.e. Langmuir and Freundlich were proposed to evaluate data. Adsorption in the Langmuir model is a monolayer process and the existence of a limited number of adsorption sites on the absorbent surface is the basis of this model. Occupying the adsorption site with a dye molecule causes further adsorption not to occur in that place because it can only keep one adsorption molecule in itself. The linear form of this model is described in Eq (3).

$$\frac{C_e}{q_e} = \frac{1}{q_m K_L} + \frac{1}{q_m} C_e \quad (3)$$

Where C_e (mg/L) is the concentration of adsorbate in the solution at the equilibrium state; q_e and q_{max} (mg/g) are the adsorption capacity at the equilibrium state and the maximum monolayer adsorption capacity of adsorbent, respectively. K_L (L/mg) is the Langmuir constant, indicating the affinity of the adsorbate. The values of q_{max} and K_L can be calculated by plotting C_e/q_e versus C_e (Fig 7a), which were obtained from the slope and intercept of the straight line, respectively. Based on the related calculation, q_{max} and K_L parameters were 84.74 mg/g and 0.0416 L/mg, respectively (Table 2).

A good fit of the experimental data with the Langmuir model can express a dimensionless constant separation factor (R_L) (Eq 4).

$$R_L = \frac{1}{1 + K_L C_0} \quad (4)$$

where R_L is the adsorption nature and C_0 (mg/L) is the maximum initial dye concentration. When $R_L = 0$, $0 < R_L < 1$, $R_L = 1$, and $R_L > 1$, the adsorption nature is irreversible, favorable, linear, and unfavorable, respectively. R_L value was found to be 0.5458, denoting favorable monolayer sorption [55,56].

The assumption of the Freundlich model is that the surface is heterogeneous and the desired analytes are adsorbed in the form of multilayer adsorption. This model is represented as follows:

$$Log\ q_e = log\ (K_F) + \frac{1}{n}\ log\ (C_e) \quad (5)$$

The constant value of the adsorption intensity and the nature of adsorption are specified by K_F and 1/n, respectively. The plot of Log q_e versus Log C_e (Fig 7) can estimate the K_F and 1/n values via slope and intercept [57]. The 1/n value was achieved at 0.5745, which shows the favorability of adsorption. The data obtained from the present study (Table 2) showed a better fit with the Langmuir model with a coefficient of determination (R^2) equal to 0.9993 for the adsorption of DR16.

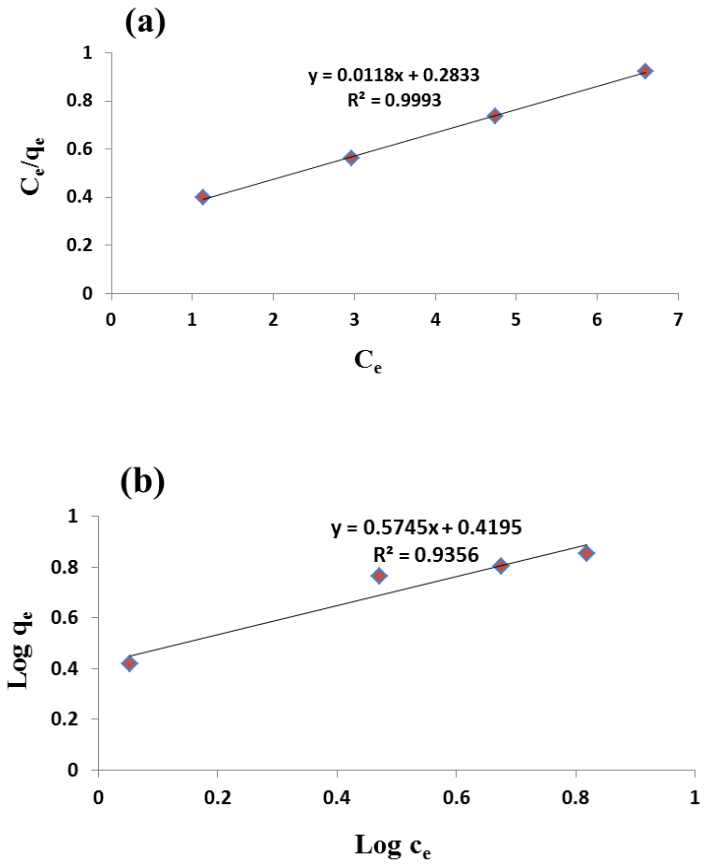

Fig 7. (a) Langmuir and (b) Freundlich isotherms in different concentrations for the removal of DR16 by CS-nZVI-Ni

Table 2. The obtained parameters of isotherm models for DR16 removal

Langmuir				Freundlich		
q_{max} (mg/g)	K_L (L/mg)	R_L	R^2	K_f	1/n	R^2
84.74	0.0416	0.5524	0.9993	2.627	0.5745	0.9356

3.4. Adsorption kinetics

In this study, Pseudo-first-order (PFO), pseudo-second-order (PSO), and Elovich were investigated to express the adsorption kinetics of DB16 onto CS-nZVI-Ni. In the PFO model, the Lagergren equation is applied to evaluate the adsorption in the solid-liquid system (Eq 6).

$$ln\,(q_e - q_t) = lnq_e - k_1(t) \quad (6)$$

Where q_t and q_e (mg/g) are the amount of the DB 86 adsorbed at time t and equilibrium state, respectively; K_1 (min^{-1}) represents the constant rate of PFO at the equilibrium state [58]. ln (q_e-q_t) versus time (min) was plotted (Fig 8a) to obtain K_1 from the slope of this plot.

In the PSO model, it is assumed that the type of process is chemical adsorption and the adsorption capacity determines the adsorption rate. Eq (7) can describe the PSO process.

$$\frac{t}{q_t} = \frac{1}{k_2 q_e^2} + \frac{t}{q_e} \quad (7)$$

Where k_2 (g mg^{-1}·min^{-1}) denotes the rate constant at the equilibrium state [59]. The linear chart of t/qt versus time (min) was plotted and q_e and K_2 parameters were found from the slope and intercept, respectively (Fig 8b). As shown, the R^2 of the PSO model fits best with the adsorption of dye onto CS-nZVI-Ni.

The Elovich equation can be described as follows:

$q_t = 1/\beta.\ln(\alpha.\beta) + 1/\beta.\ln(t)$ (8)

Herein α (mg/g/min) is the initial adsorption rate and β (g/mg) is assigned to the extent of surface coverage and activation energy for chemisorption [60-62].

The parameters related to the mentioned models were calculated and given in Table 3.

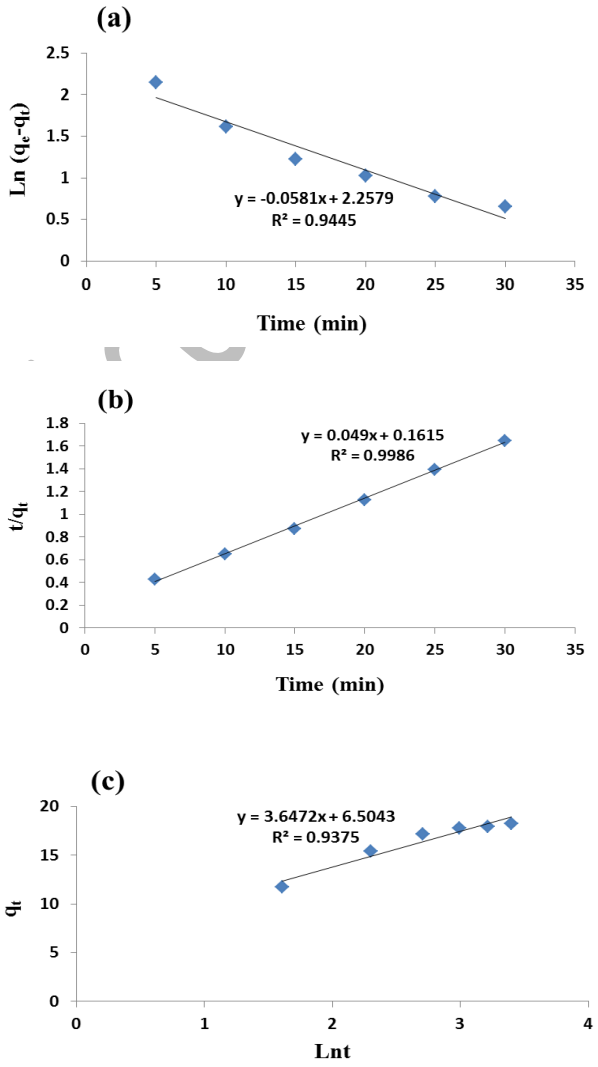

Fig 8. (a) Pseudo-first-order, (b) Pseudo-second-order, and (c) Elovich adsorption kinetics of DR16

Table 3. The obtained kinetic parameters for DB 86 removal

Kinetic	Parameters	
Pseudo-first-order	K_1 (min^{-1})	0.0581
	q_e (mg g^{-1})	9.562
	R^2	0.9445
Pseudo-second-order	K_2 (g.mg^{-1}. min^{-1})	0.0148
	q_e (mg g^{-1})	20.40
	R^2	0.9986
Elovich	α (mg/g/min)	0.2498
	β (g/mg)	0.2741
	R^2	0.9375

3.5. Thermodynamic studies

The determination of the spontaneous process was evaluated using a thermodynamic study. Parameters of thermodynamics, including the adsorption Gibbs free energy (ΔG^0), standard enthalpy (ΔH^0), and standard entropy (ΔS^0) were calculated through the adsorption isotherm of the DR16 onto the CS-nZVI-Ni at different temperatures (283, 298, 323 K). These parameters were calculated using equations (9) to (12).

$$\Delta G^0 = -RTlnK \quad (9)$$

$$K = {}^{q_e}/_{c_e} \quad (10)$$

$$lnK = -\frac{\Delta H^0}{RT} + \frac{\Delta S^0}{R} \quad (11)$$

$$\Delta G^0 = \Delta H^0 - T\Delta S^0 \quad (12)$$

where K is the thermodynamic equilibrium constant; R (8.3145 J mol^{-1} K^{-1}) is the gas constant; T (K) is the absolute temperature; q_e is the adsorption capacity and C_e is the equilibrium concentration of pollutant. The ΔH^0 and ΔS^0 values were determined via the slope and intercept of the equation of the Van't Hoff plot (Lnk versus 1/T) (Fig 9), respectively. The negative value of ΔG^0 confirms the spontaneous nature of the adsorption process, as well as the negative value of ΔH^0 proves the exothermic reaction (Table 4).

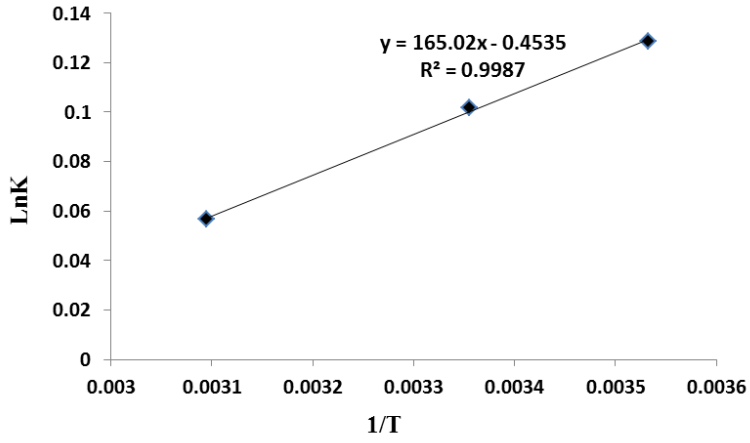

Fig 9. LnK versus 1/T for the removal of DR16 by CS-nZVI-Ni

Table 4. Thermodynamic parameters of DR16 adsorption onto CS-nZVI-Ni at different temperatures

ΔG^0 (J/mol)			ΔH^0 (J/mol)	ΔS^0 (J/mol K)
283 K	298 K	323 K		
−302.57	−251.72	−151.99	−1373.97	−3.77

3.6. Reusability of adsorbent

Costs and waste production can be reduced by adsorbent recycling. Therefore, the removal efficiency of the proposed adsorbent versus five successive cycles was studied. As shown in Fig 10, it can be concluded that CS-nZVI-Ni has a high potential after five removal processes for reuse. The removal percentage was diminished from 88.32% to 60.28%.

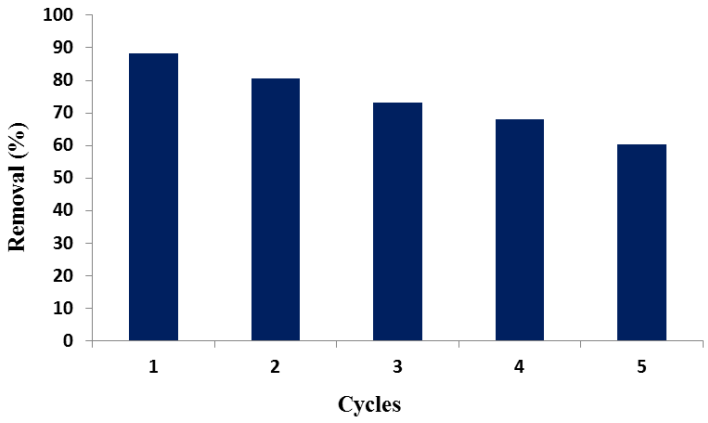

Fig 10. Reusability of CS-nZVI-Ni for the removal of DR16

3.7. Selectivity

The influence of interfering substances like Na^+, Mg^{2+}, Fe^{2+}, Fe^{3+}, and so on was evaluated to estimate DR16. Table 5 indicated that interfering ions did not remarkably affect the determination of the mentioned dye. The

permissible concentration of these interfering substances is higher than the DR16 concentration, representing a proper selectivity between dye and other substances.

Table 5. Interfering effect of several species for the determination of DR16

Species	Tolerance limit [X]/[DR16]
Na^+, Cl^-, K^+, NO^{3-}, CO_3^{2-}	300
Ni^{2+}, Fe^{3+}	100
Fe^{2+}, SO_4^{2-}	500
Mg^{2+}, Zn^{2+}	50

3.8. Comparative study

The performance of some previously reported adsorbents is compared to the results of this study (Table 3). The studied adsorbent (CS-nZVI-Ni) considerably outperforms other sorbents in terms of the q_{max}, removal percentage, and contact time. The adsorbent namely B-ZnO/TiO_2 reveals a removal efficiency of 100% with a contact time of 200 min. This contact time is higher than the contact time of this study (15 min). The q_{max} values of all adsorbents are lower than qmax of CS-nZVI-Ni (84.74 mg/g). As a result, the proposed adsorbent seems to have a bright future in widespread practical usage.

Table 3. Comparison of various studies for the removal of different dyes

Adsorbent	Pollutant	q_{max} (mg/g)	Removal efficiency (%)	Time (min)	Ref.
B-ZnO/TiO_2	DR16	13.05	100.00	200	[4]
Ag NPs/Ag_3VO4/$AgVO_3$/GO	DR16	---	61.54	155	[5]
Feldspar	DR16	5.30	93.00	15	[63]
Acidic soil containing iron	DR81[1]	---	84.00	30	[64]
ZFN-CTAB[2]	DR23[3]	26.10	63.00	60	[65]
CS-nZVI-Ni	DR16	84.74	98.59	15	Present study

[1] Direct Red 81

[2] Zinc ferrite nanoparticle (ZFN)- cetyl trimethylammonium bromide (CTAB)

[3] Direct Red 23

3.9. Economic assessment

An appraisal related to the cost of using CS-nZVI-Ni for the adsorption of DR16 was carried out based on the saturation capacity (84.74 mg/g) of the CS-nZVI-Ni alone, without considering other cost factors. Other researchers also have used this way to compute the adsorption process cost [66]. The adsorption system cost was considered as the relative cost for the adsorption of 1 g of DR16. Every 0.2 g of adsorbent can remove 1 g of DR16 with a cost of 0.3 USD, which can be said to be an economical adsorbent.

3.10. Adsorption mechanism

The removal mechanism of synthesized NPs along with CS was via the degradation catalyzed by Fe° and adsorption caused by iron oxide shell and CS. The nZVI particles can destroy the DR16 molecule chromophore using atomic hydrogen which was generated by the reaction between Fe° and H_2O and H^+. Ni located on the surface of Fe° has a catalyst role, which facilitates the production of atomic hydrogen and enables electron transfer through the iron oxide shell. Therefore, Fe/Ni nanoparticles are stimulated for higher dye removal efficiency. CS as a stabilizer not only preserves the nZVI particles and enhances the interaction between Fe° and DR16 but also reveals a synergetic effect on the removal of DR16 by the adsorption process (Scheme 2) [53].

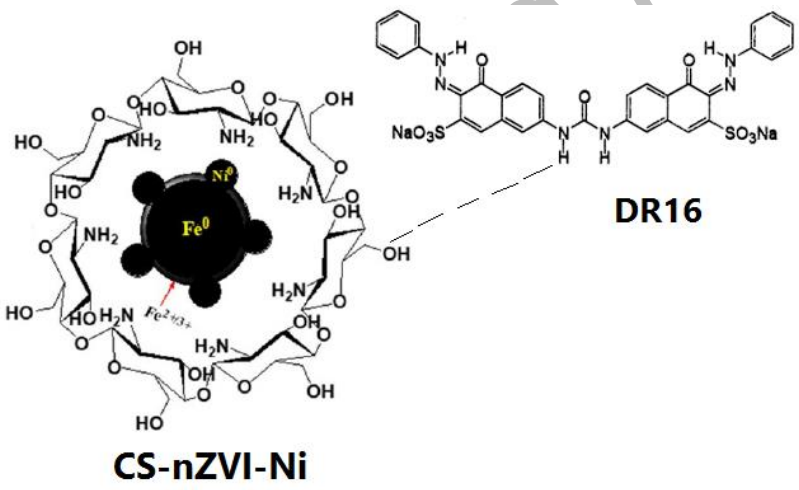

Scheme 2. Mechanism of raction between CS-nZVI-Ni and DR16

4. Conclusion

This study indicates the removal of an azo dye, Direct Red 16, using nZVI-Ni bimetallic nanoparticles along with chitosan from an aqueous solution. The successful synthesis of CS-nZVI-Ni was confirmed by SEM, EDX, FTIR, XRD, BET, and VSM analysis. The effect of experimental factors, including pH, adsorbent dosage, contact time, and initial concentration of dye was studied to obtain the highest removal efficiency. Interpretation of experimental data was better with the Langmuir model. Among the various kinetic models (Pseudo-first-order, pseudo-second-order, and Elovich), the adsorption kinetic results revealed that the data followed the pseudo-second-order model. Adsorption thermodynamic parameters indicated that the adsorption of DR16 on the surface of CS-nZVI-NI was exothermic and spontaneous. The reusability of the adsorbent demonstrated that the dye removal was reached to 60.28% after five recycles. In future studies, the synthesized adsorbent can be used to remove other azo dyes from

the effluents of different factories. To reach the dye wastewater treatment, an adsorption method with CS-nZVI-Ni as a simple, low-cost, available, and efficient adsorbent would be a viable option.

References

[1] Arif, M., Catalytic degradation of azo dyes by bimetallic nanoparticles loaded in smart polymer microgels, RSC Adv. **13**: 3008–3019 (2023).

[2] Mousavi, S.M., Meraji, S.H., Sanati, A.M., Ramavandi, B., Phenol red dye removal from wastewater using TiO_2-FSM-16 and Ni-FSM-16 photocatalysts, Heliyon. 9: e14488 (2023).

[3] Karbul, A., Mohammadi, M.K., Jalilzadeh Yengejeh, R., Farrokhian, F., Nanocomposite Fe-Co-V/Zeolite: Highly Efficient Composite for Removal of Methyl Orange Dye, J. Environ. Health Sci. Eng. **10**: 149-159 (2022).

[4] Abdulmunem Habeeb, S., Zinatizadeh, A.A., Zangeneh, H., Photocatalytic Decolorization of Direct Red16 from an Aqueous Solution Using B-ZnO/TiO_2 Nano Photocatalyst: Synthesis, Characterization, Process Modeling, and Optimization, Water. **15**: 1203 (2023).

[5] Hazizadeh Fard, B., Ranjineh Khojasteh, R., Gharbani, P., Photocatalytic Degradation of Direct Red 16 Dye using Ag/Ag_3VO_4/$AgVO_3$/GO Nanocomposite, S. Afr. J. Chem. **73**: 1-6 (2023).

[6] Umar, A., Sufaid Khan, M., Alam, S., Zekker, I., Burlakovs, J., dC Rubin, S.S., Dhar Bhowmick, G., Kallistova, A., Pimenov, N., Zahoor, M., Synthesis and Characterization of Pd-Ni Bimetallic Nanoparticles as Efficient Adsorbent for the Removal of Acid Orange 8 Present in Wastewater, Water. **13**: 1095 (2021).

[7] Ahmed, I.A., Nosier, S.A., Malash, G.F., Hussein, M., Abdel-Aziz, M.H., Sedahmed, G.H., Fathalla, A.S., Removal of Brilliant Yellow Azo Dye from Wastewater by Electrocoagulation in a Cell of Improved Design, Water, Air, & Soil Pollut. **237**: 112 (2023).

[8] Wang, W., Chen, Z., Wu, K., Liu, Z., Yang, S., Yang, Q., Dzakpasu, M., Coagulation performance of cucurbit[8]uril for the removal of azo dyes: effect of solution chemistry and coagulant dose, Water Sci. Technol. **78**: 415–423 (2018).

[9] Han, G., Du, Y., Huang, Y., Wang, W., Su, S., Liu, B., Study on the removal of hazardous Congo red from aqueous solutions by chelation flocculation and precipitation flotation process, Chemosphere. **289**: 133109 (2022).

[10] Ezzahra Titchou, F., Zazou, H., Afanga, H., El Gaayda, J., Ait Akbour, R., Hamdani, M., Oturan, M.A., Electro-Fenton process for the removal of Direct Red 23 using BDD anode in chloride and sulfate media, J. Electroanal. Chem. **897**: 115560 (2021).

[11] Li, J., Zhu, K., Li, R., Fan, X., Lin, H., Zhang, H., The removal of azo dye from aqueous solution by oxidation with peroxydisulfate in the presence of granular activated carbon: Performance, mechanism and reusability, Chemosphere. **259**: 127400 (2020).

[12] Dadban Shahamat, Y., Masihpour, M., Borghei, P., Rahmati, S.H., Removal of azo red-60 dye by advanced oxidation process O_3/UV from textile wastewaters using Box-Behnken design, Inorg. Chem. Commun. **143**: 109785 (2022).

[13] Yousefinia, Sh., Sohrabi, M.R., Motiee, F., Davallo, M., Enhanced simultaneous removal of direct red 81 and bisphenol A from aqueous media by coupling nano zero-valent iron (nZVI) particles with graphene oxide and copper: Isotherm and kinetic adsorption studies, Mater. Chem. Phys. **296**: 127206 (2023).

[14] Yeoh, J.X., Jamil, S., Syukri, F., Koyama, M., Mobarekeh, M.N., Comparison between Conventional Treatment Processes and Advanced Oxidation Processes in Treating Slaughterhouse Wastewater: A Review, Water. **14**: 3778 (2022).

[15] Ebba, M., Asaithambi, P., Alemayehu, E., Development of electrocoagulation process for wastewater treatment: optimization by response surface methodology, Heliyon. **8**: e09383 (2022).

[16] Ullah Jan, S., Ahmad, A., Ali Khan, A., Melhi, S., Ahmad, I., Sun, G., Chen, C.M., Ahmad, R., Removal of azo dye from aqueous solution by a low-cost activated carbon prepared from coal: adsorption kinetics, isotherms study, and DFT simulation, Environ. Sci. Pollut. Res. **28**: 10234–10247 (2021).

[17] Li, Z., Ren, D., Wang, Z., Jiang, S., Zhang, S., Zhang, X., Chen, W., Adsorption and removal of direct red 31 by Cu-MOF: optimization by response surface, Water Sci. Technol. **86**: 80–94 (2022).

[18] Ashrafi, M., Bagherian, G., Arab Chamjangali, M., Goudarzi, N., Removal of Brilliant Green and Crystal violet from Mono- and Bi-component Aqueous Solutions Using NaOH-modified Walnut Shell, Anal. Bioanal. Chem. Res. **5**: 95-114 (2018).

[19] Si, J., Yang, X., Luan, H., Shao, Y., Yao, K., Cheap, fast and durable degradation of azo dye wastewater by zero-valent iron structural composites, J. Environ. Chem. Eng. **9**: 106314 (2021).

[20] Jiang, D., Huang, D., Lai, C., Xu, P., Zeng, G., Wan, J., Tang, L., Dong, H., Huang, B., Hu, T., Difunctional chitosan-stabilized Fe/Cu bimetallic nanoparticles for removal of hexavalent chromium wastewater, Sci. Total Environ. **644**: 1181–1189 (2018).

[21] Safinejad, A., Goudarzi, N., Arab Chamjangali, M., Bagherian, G., Effective simultaneous removal of Pb(II) and Cd(II) ions by a new magnetic zeolite prepared from stem sweep, Mater. Res. Express. **4**: 116104 (2017).

[22] Vuong, N.M., Nguyen, P.T., Kim Oanh Nguyen, T., Binh Nguyen, D., My-Dieu Tran, T., Thi Kim Oanh, L., Nguyen, T.B., Thi Pham, T., Yi Andrew Lin, K., Bui, X.T., Application of nano zero-valent iron particles coated by carboxymethyl cellulose for removal of Congo red dye in aqueous solution, Case Stud. Chem. Environ. Eng. **8**: 100469 (2023).

[23] Foster, S.L., Estoque, K., Voecks, M., Rentz, N., Greenlee, L.F., Removal of Synthetic Azo Dye Using Bimetallic Nickel-Iron Nanoparticles, J. Nanomater. **2019**: 1-12 (2019).

[24] Bokare, A.D., Chikate, R.C., Rode, C.V., Paknikar, K.M., Iron-nickel bimetallic nanoparticles for reductive degradation of azo dye Orange G in aqueous solution, Appl. Catal. B: Environmental. **79**: 270–278 (2008).

[25] Aparecida Gonçalves, A., França Araújo, A., José Mendes Pires, M., Moreira Verly, R., Vilela Franco, D., Morais da Silva, L., Synthesis of chitosan-stabilised iron and nickel nanoparticles and the application in the reductive degradation of nimesulide, Eclética Química Journal. **43**: 10-25 (2018).

[26] Yazdanbakhsh, A.R., Daraei, H., Rafiee, M., Kamali, H., Performance of iron nano particles and bimetallic Ni/Fe nanoparticles in removal of amoxicillin trihydrate from synthetic wastewater, Water Sci. Technol. **73**: 2998-3007 (2016).

[27] Xie, Y., Xie, S., Yang, H., Deng, Y., Qian, H., Zeng, X., A dramatically improved degradation efficiency of azo dyes by zero valent iron powders decorated with in-situ grown nanoscale Fe_2B, J. Alloys Compd. **842**: 155818 (2020).

[28] Keshipour, S., Mirmasoudi, S.S., Chitosan supported bimetallic Pd/Co nanoparticles as a heterogeneous catalyst for the reduction of nitroaromatics to amines, Adv. Environ. Tech. **1**: 59-65 (2017).

[29] Ali, F., Bahadar Khan, S., Kamal, T., Alamry, K.A., Asiri, A.M., Chitosan-titanium oxide fibers supported zero-valent nanoparticles: Highly efficient and easily retrievable catalyst for the removal of organic pollutants, Sci. Rep. **8**: 6260 (2018).

[30] Elzahar, M.M.H., Bassyouni, M., Removal of direct dyes from wastewater using chitosan and polyacrylamide blends, Sc. Rep. **13**: 15750 (2023).

[31] Rashid, S., Shen, C., Chen, X., Li, S., Enhanced catalytic ability of chitosan-Cu-Fe bimetal complex for the removal of dyes in aqueous solution, RSC Adv. **5**: 90731-90741 (2015).

[32] Asgari, G., Ramavandi, B., Farjadfard, S., Abatement of Azo Dye from Wastewater Using Bimetal-Chitosan, Sci. World J. **2013**: 1-11 (2013).

[33] Neolaka, Y., Lawa, Y., Naat, J., Lalang, A.G., Widyaningrum, B., Ngasu, G.F., Niga, K., Darmokoesoemo, H., Iqbal, M., Kusuma, H., Adsorption of methyl red from aqueous solution using Bali cow bones (*Bos javanicus domesticus*) hydrochar powder, Results Eng. **17**: 100824 (2023).

[34] Khera, R., Iqbal, M., Ahmad, A., Hassan, S., Nazir, A., Kausar, A., Kusuma, H., Niasr, J., Masood, N., Younas, U., Nawaz, R., Khan, M., Kinetics and equilibrium studies of copper, zinc, and nickel ions adsorptive removal on to Archontophoenix alexandrae: conditions optimization by RSM, Desalin Water Treat. **201**: 289–300 (2020).

[35] Kuncoro, E.P., Mitha Isnadina, W.R., Darmokoesoemo, H., Dzembarahmatiny, F., Kusuma, H.S., Characterization and isotherm data for adsorption of Cd^{2+} from aqueous solution by adsorbent from mixture of bagasse-bentonite, Data in Brief. **16**: 354–360 (2018).

[36] Kuncoro, E.P., Mitha Isnadina, D.R., Darmokoesoemo, H., Fauziah, O., Kusuma, H.S., Characterization, kinetic, and isotherm data for adsorption of Pb^{2+} from aqueous solution by adsorbent from mixture of bagasse-bentonite, Data in Brief. **16**: 622–629 (2018).

[37] Kuncoro, E.P., Soedarti, T., CaturPutranto, T.W., Putranto, C., Darmokoesoemo, H., RizkiAbadi, N., Kusuma, H., Characterization of amixture of algae waste-bentonite used as adsorbent for the removal of Pb^{2}_{+} from aqueous solution, Data in Brief. **16**: 908–913 (2018).

[38] Smiley, E., Tadayon, F., Sohrabi, M.R., Vitamin B2 Removal from Aqueous Solution Using Magnetic Nanoparticles/ Orange Peel Composite: Optimization Using Response Surface Methodology, Iran. J. Chem. Chem. Eng. **41**: 3706-3717 (2022).

[39] Yasmeen, S., Kanti Kabiraz, M., Saha, B., Qadir, R., Gafur, A., Masum, S., Chromium (VI) Ions Removal from Tannery Effluent using Chitosan-Microcrystalline Cellulose Composite as Adsorbent, Int. Res. J. Pure Appl. Chem. **10**: 1-14 (2016).

[40] Ahmadi, M., Foladivanda, M., Jafarzadeh, N., Ramavandi, B., Jorfi, S., Kakavandi, B., Synthesis of chitosan zero-valent iron nanoparticlessupported for cadmium removal: characterization, optimization and modeling approach, J. Water Supply: Res. Technol. - AQUA. **66**: 116–130 (2017).

[41] Boudouaia, N., Bengharez, Z., Jellali, S., Preparation and characterization of chitosan extracted from shrimp shells waste and chitosan film: application for Eriochrome black T removal from aqueous solutions, Appl. Water Sci. **9**: 91 (2019).

[42] Rose Puthukkara, A., Jose, S., lal, D., Chitosan stabilized Fe/Ni bimetallic nanoparticles for the removal of cationic and anionic triphenylmethane dyes from water, Environ. Nanotechnol. Monit. Manag. **14**: 100295 (2020).

[43] Kumar Sharma, A., Desnavi, S., Dixit, C., Varshney, U., Sharma, A., Extraction of Nickel Nanoparticles from Electroplating Waste & their application in production of Bio-Diesel from Biowaste, Int. J. Chem. Eng. Appl. **6**: 3 (2014).

[44] He, S., Zhu, F., Li, L., Ren, W., Box–Behnken design for the optimization of the removal of Cr(VI) in soil leachate using nZVI/Ni bimetallic particles, Soil Sediment Contam: An International Journal. **27**: 658–673 (2018).

[45] Ali, F., Bahadar Khan, S., Kamal, T., Alamry, K.A., Asiri, A.M., Sobahi, T.R.A., Chitosan coated cotton cloth supported zero-valent nanoparticles: Simple but economically viable, efficient and easily retrievable catalysts, Sci Rep. **7**: 16957 (2017).

[46] Shan, A., Farooq, U., Lyu, S., Qamar Zaman, W., Abbas, Z., Ali, M., Idrees, A., Tang, P., Li, M., Sun, Y., Sui, Q., Efficient removal of trichloroethylene in surfactant amended solution by nano Fe^0-Nickel bimetallic composite activated sodium persulfate process, Chem. Eng. J. **386**: 123995 (2019).

[47] Van der Horsta, C., Silwanaa, B., Makombea, M., Iwuohab, E., Somerseta, V., Application of a chitosan bimetallic nanocomposite for the simultaneous removal of cadmium, nickel, and lead from aqueous solution, Desalin and Water Treat. **220**: 168–181 (2021).

[48] Amiri, Sh., Sohrabi, M.R., Motiee, F., Optimization Removal of the Ceftriaxone Drug from Aqueous Media with Novel Zero-Valent Iron Supported on Doped Strontium Hexaferrite Nanoparticles by Response Surface Methodology, ChemistrySelect. **5**: 5831 –5840 (2020).

[49] Toutounchi, S., Shariati, Sh., Mahanpoor, K., Synthesis of nano-sized magnetite mesoporous carbon for removal of Reactive Yellow dye from aqueous solutions, Appl. Organomet. Chem. **23**: e5046 (2019).

[50] Thommes, M., Kaneko, K., Neimark, A.V., Olivier, J.P., Rodriguez-Reinoso, F., Rouquerol, J., Sing, K.S.W., Physisorption of gases, with special reference to the evaluation of surface area and pore size distribution (IUPAC Technical Report), Pure Appl. Chem. **87**: 1051-1069 (2015).

[51] Neolaka, A.B., Lawa, Y., Naat, J., Riwu, A.P., Lindu, E., Darmokoesoemo, H., Widyaningrum, B., Iqbal, M., Kusuma, H., Evaluation of magnetic material IIP@GO-Fe_3O_4 based on Kesambi wood (*Schleichera oleosa*) as a potential adsorbent for the removal of Cr(VI) from aqueous solutions, React Funct Polym. **166**: 105000 (2021).

[52] Neolaka, A.B., Lawa, Y., Naat, J., Riwu, A., Mango, A., Darmokoesoemo, H., Widyaningrum, B., Iqbal, M., Kusuma, H., Efficiency of activated natural zeolite-based magnetic composite (ANZ-Fe_3O_4) as a novel adsorbent for removal of Cr(VI) from wastewater, J. Mater. Res. Technol. **18**: 2896-2909 (2022).

[53] Anju Rose Puthukkara, P., Sunil Jose, T., Dinoop lal, S., Chitosan stabilized Fe/Ni bimetallic nanoparticles for the removal of cationic and anionic triphenylmethane dyes from water, Environ. Nanotechnol. Monit. Manag. **14**: 100295 (2020).

[54] Ahmed, I.A., Hussein, H.S., ALOthman, Z.A., ALanazi, A.G., Salem Alsaiari, N., Khalid, A., Green Synthesis of Fe–Cu Bimetallic Supported on Alginate-Limestone Nanocomposite for the Removal of Drugs from Contaminated Water, Polymers. **15**: 1221 (2023).

[55] Myneni, V.R., Kanidarapu, N.R., Vangalapati, M., Methylene Blue Adsorption by Magnesium Oxide Nanoparticles Immobilized with Chitosan (CS-MgONP): Response Surface Methodology, Isotherm, Kinetics and Thermodynamic Studies, Iran. J. Chem. Chem. Eng. **39**: 29-42 (2020).

[56] Myneni, V.R., Kanidarapu, N.R., Shaik, F., Vanalapati, M., Response Surface Modeling of the Removal of Methyl Orange Dye from an Aqueous Solution Using Magnesium Oxide Nanoparticles Immobilized on Chitosan, Iran. J. Chem. Chem. Eng. 41 (2022) 1602-1618.

[57] Alswieleh, A.M., Efficient Removal of Dyes from Aqueous Solution by Adsorption on L-Arginine-Modified Mesoporous Silica Nanoparticles, Processes. **10**: 1079 (2022).

[58] Neolaka, Y., Lawa, Y., Naat, J.N., Pau Riwu, A.A., Darmokoesoemo, H., Supriyanto, G., Holdsworth, G.I., Amenaghawon, A.N., Kusuma, H.S., A Cr(VI)-imprinted-poly(4-VP-co-EGDMA) sorbent prepared using precipitation polymerization and its application for selective adsorptive removal and solid phase extraction of Cr(VI) ions from electroplating industrial wastewater, React Funct Polym. **147**: 104451 (2020).

[59] Naat, J.N., Neolaka, Y., Lapailaka, T., Triandi, R., Sabarudin, A., Darmokoesoemo, H., Septya Kusuma, H., Adsorption of Cu(II) and Pb(II) using silica@mercapto (HS@M) hybrid adsorbent synthesized from silica of takari sand: Optimization of parameters and kinetics, Rasayan J. Chem. **40**: 550-560 (2021).

[60] Neolaka, Y., Lawa, Y., Naat, J., Riwu, A., Darmokoesoemo, H., Ayu Widyaningrum, B., Iqbal, M., Kusuma, H., Indonesian Kesambi wood (Schleichera oleosa) activated with pyrolysis and H_2SO_4 combination methods to produce mesoporous activated carbon for Pb(II) adsorption from aqueous solution, Environ. Technol. Innov. **24**: 101997 (2021).

[61] Neolaka, Y., Supriyanto, G., Darmokoesoemo, H., Kusuma, H., Adsorption performance of Cr(VI)-imprinted poly(4-VP-co-MMA) supported on Activated Indonesia (Ende-Flores) natural zeolite structure for Cr(VI) removal from aqueous solution, J. Environ. Chem. Eng. **6**: 3436-3443 (2018).

[62] Neolaka, Y., Lawa, Y., Naat, J., Riwu, A., Iqbal, M., Darmokoesoemo, H., Kusuma, H., The adsorption of Cr(VI) from water samples using graphene oxide-magnetic (GO-Fe_3O_4) synthesized from

natural cellulose-based graphite (kusambi wood or Schleichera oleosa): Study of kinetics, isotherms and thermodynamics, J. Mater. Res. Technol. **9**: 6544-6556 (2020).

[63] Jamil, N., Maqsood Khan, S., Ahsan, N., Anwar, J., Qadir, A., Zameer, M., Shafique, U., Removal of Direct Red 16 (Textile Dye) from Industrial Effluent by using Feldspar, J. Chem. Soc. Pak. **36**: 191-197 (2014).

[64] Shahsavani, S., Dehghani, M., Shamsedini, N., Removal of Direct Red 81 from Aqueous Solution Using an Acidic Soil Containing Iron (Case Study of Lahijan Soil), Iran. J. Chem. Chem. Eng. **38**: 107-112 (2019).

[65] Mohammad Mahmoodi, N., Abdi, J., Bastani, D., Direct dyes removal using modified magnetic ferrite nanoparticle, J. Environ. Health Sci. Eng. **12**: 96 (2014).

[66] Soni, S., Kumar Bajpai, P., Bharti, D., Bharti, J., Arora, C., Removal of crystal violet from aqueous solution using iron based metal organic framework, Desalin and Water Treat. **205**: 386–399 (2020).